

Article

Measurements and Modelling of Thermally Induced Warpings of DIMM Socket Server PCB Assembly after Solder Reflow Processes

Ming-Yi Tsai ^{1,*} , Yu-Wen Wang ¹, Yen-Jui Lu ¹, Tzu-Min Lu ² and Shu-Tan Chung ²

¹ Department of Mechanical Engineering, Chang Gung University, Taoyuan 33302, Taiwan; wanglovedog@gmail.com (Y.-W.W.); randy12226@gmail.com (Y.-J.L.)

² Inventec Corporation, Taoyuan 333547, Taiwan; liu.lawrence@inventec.com (T.-M.L.); chung.kelvin@inventec.com (S.-T.C.)

* Correspondence: mytsai@mail.cgu.edu.tw

Abstract: The thermal warpage of a server-computer-used DIMM socket-PCB assembly after the solder reflow process is studied experimentally, theoretically, and numerically, especially along the socket lines and over the entire assembly. Strain gauge and shadow moiré are used for determining the coefficients of thermal expansion of the PCB and DIMM sockets and for measuring the thermal warpings of the socket-PCB assembly, respectively, while a newly proposed theory and a finite element method (FEM) simulation are used to calculate the thermal warpage of the socket-PCB assembly in order to understand its thermo-mechanical behavior and then further identify some important parameters. The results show that the theoretical solution validated by the FEM simulation provides the mechanics with the critical parameters. In addition, the cylindrical-like thermal deformation and warpage, measured by the moiré experiment, are also consistent with the theory and FEM simulation. Moreover, the results of the thermal warpage of the socket-PCB assembly from the strain gauge suggest a warpage dependence on the cooling rate during the solder reflow process, due to the nature of the creep behavior in the solder material. Finally, the thermal warpings of the socket-PCB assemblies after the solder reflow processes are provided through a validated FEM simulation for future designs and verification.

Keywords: thermal warpage; DIMM socket; printed circuit board; strain gauge; shadow moiré; finite element method



Citation: Tsai, M.-Y.; Wang, Y.-W.; Lu, Y.-J.; Lu, T.-M.; Chung, S.-T.

Measurements and Modelling of Thermally Induced Warpings of DIMM Socket Server PCB Assembly after Solder Reflow Processes.

Materials **2023**, *16*, 3233. <https://doi.org/10.3390/ma16083233>

Academic Editor: Alexander N. Obratsov

Received: 9 February 2023

Revised: 11 April 2023

Accepted: 12 April 2023

Published: 19 April 2023



Copyright: © 2023 by the authors. Licensee MDPI, Basel, Switzerland. This article is an open access article distributed under the terms and conditions of the Creative Commons Attribution (CC BY) license (<https://creativecommons.org/licenses/by/4.0/>).

1. Introduction

The thermally induced warpings of integrated-circuit (IC) package- or component-PCB (printed circuit board) assemblies after the solder reflow processes, due to the mismatch of the coefficients of thermal expansion (CTEs) of those packages or components with the PCB, create problems in the later-on assembly and the solder joint reliability under in-service thermal cycling [1]. Therefore, measurement and analysis approaches to this problem are of importance and needed in order to provide further control and reduction in the thermal warpage of the package- or component-PCB assembly after the reflow processes. Reliable and easy-to-use strain gauges [2] have been used in measuring the mechanical strains on PCBs and packages [3] and on the CPU assembly [4], as well as the thermally induced curvatures and warpings of the PCB [5], flip-chip, and 2.5 D IC packages [6]. Additionally, a shadow moiré method [7–9] for measuring the full-field out-of-plane deformations of the specimens has been also used for the PBGA packages under thermal loading [10–12]. Both well-developed experimental methods will be applied in this study as well. The configuration and detailed geometry of a dual in-line memory module (DIMM) socket-PCB assembly used in a server computer system is shown for this study in Figure 1, including a socket for the DIMM in Figure 1a with 288 Cu pins, a socket-PCB assembly with 24 DIMM

sockets in Figure 1b representing the full-assembly specimen of interest, and a solder joint of a Cu pin for the DIMM socket on the PCB in Figure 1c. Excessive thermal warpage of the DIMM socket-PCB assembly after the solder reflow processes could generate assembly and reliability problems. The problems include the difficulty of a latch engagement and the shift of contact points with gold fingers in the DIMM socket, and a later-on installation with a flat metal plate on the full socket-PCB assembly during structural reinforcement. Therefore, the thermal warpage of the DIMM socket-PCB assembly along the socket lines and over the entire assembly after the solder reflow process will be thoroughly investigated experimentally, theoretically, and numerically in this study.

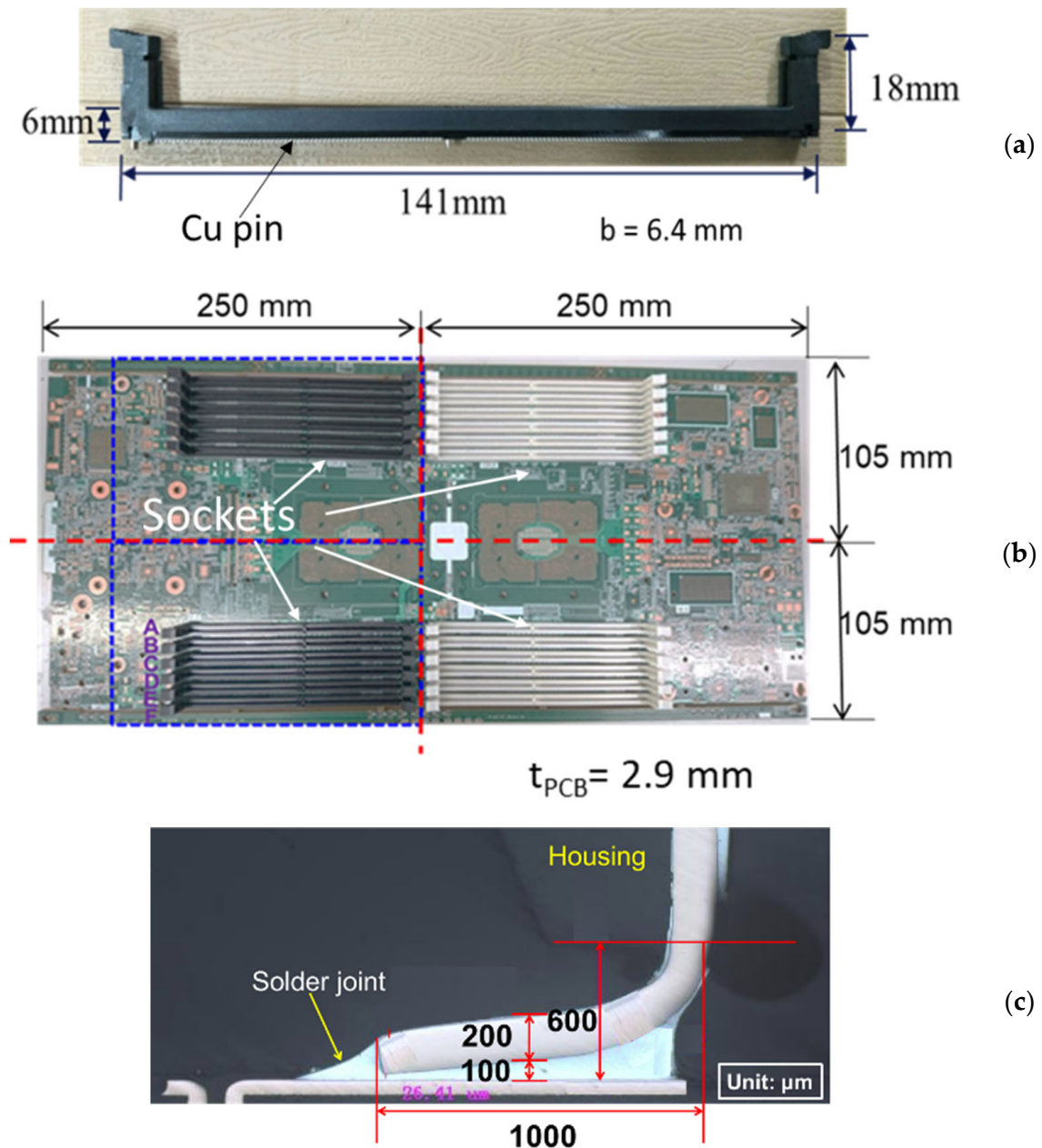


Figure 1. Configurations of (a) a DIMM socket with 288 Cu pins and width of 6.4 mm, (b) a socket-PCB assembly with 24 sockets (a full assembly), and (c) a detailed solder joint of a Cu pin for the DIMM socket on the PCB.

2. Methodologies

The methods used in this study include experimental measurements and theoretical and finite element analyses. In the experimental measurements, strain gauge and shadow moiré were used for determining the CTEs of the PCB and DIMM socket as well as for measuring thermal warpages of the socket-PCB assembly, respectively, while theoretical and finite element analyses were used to calculate the thermal warpage of the socket-PCB assembly and further identify important parameters in order to understand its thermo-mechanical behavior. These methods will be briefly illustrated in this section.

2.1. CTE and Thermal Deformation Measurement by Strain Gauges

The typical strain gauge measurement [2] at elevated temperatures can be given as

$$\varepsilon_a = \varepsilon_t + \frac{(\gamma_g + \gamma_w)}{S_g} \Delta T \quad (1)$$

where ε_a is an apparent strain which is directly obtained from a strain gauge measurement system, ε_t is a true strain which is an actual strain on the measured point of the specimen, S_g is a gauge factor, ΔT is thermal loading, and γ_g and γ_w are the temperature coefficients of resistivity of gauge grid metal material and connected lead wire, respectively.

For measuring the thermal strains of the PCB during the heating and cooling processes, back-to-back strain gauges were adhered at a specific position on both the top and bottom surfaces of the PCB. The apparent strains on the top and bottom surfaces ($\varepsilon_{a,top}$ and $\varepsilon_{a,bot}$) of the PCB can be described individually in terms of the true strains on the top and bottom surfaces ($\varepsilon_{t,top}$ and $\varepsilon_{t,bot}$) as

$$\varepsilon_{a,top} = \varepsilon_{t,top} + \frac{(\gamma_g + \gamma_w)}{S_g} \Delta T \quad (2)$$

$$\varepsilon_{a,bot} = \varepsilon_{t,bot} + \frac{(\gamma_g + \gamma_w)}{S_g} \Delta T \quad (3)$$

The strain data at various temperatures can be further converted into the bending strains (ε_b) and bending curvatures (k) of the PCB by Equations (4) and (5), respectively.

$$\varepsilon_b = (\varepsilon_{a,bot} - \varepsilon_{a,top})/2 = (\varepsilon_{t,bot} - \varepsilon_{t,top})/2 \quad (4)$$

$$k = 2\varepsilon_b/t = (\varepsilon_{t,bot} - \varepsilon_{t,top})/t \quad (5)$$

where t is the PCB thickness. Then, the out-of-plane displacement (deformation) w of the PCB under different temperatures can be further determined by Equation (6) with a given curvature k and distance x from the center.

$$w = kx^2/2 \quad (6)$$

As for the CTE measurement of the DIMM socket, the thermally induced strains across the thickness of the socket shown in Figure 2 consist of free thermal strain ε_α from thermal expansion and pure bending strains (ε_b and ε'_b) from the curvatures in the x- and y-axis (k_x and k_y).

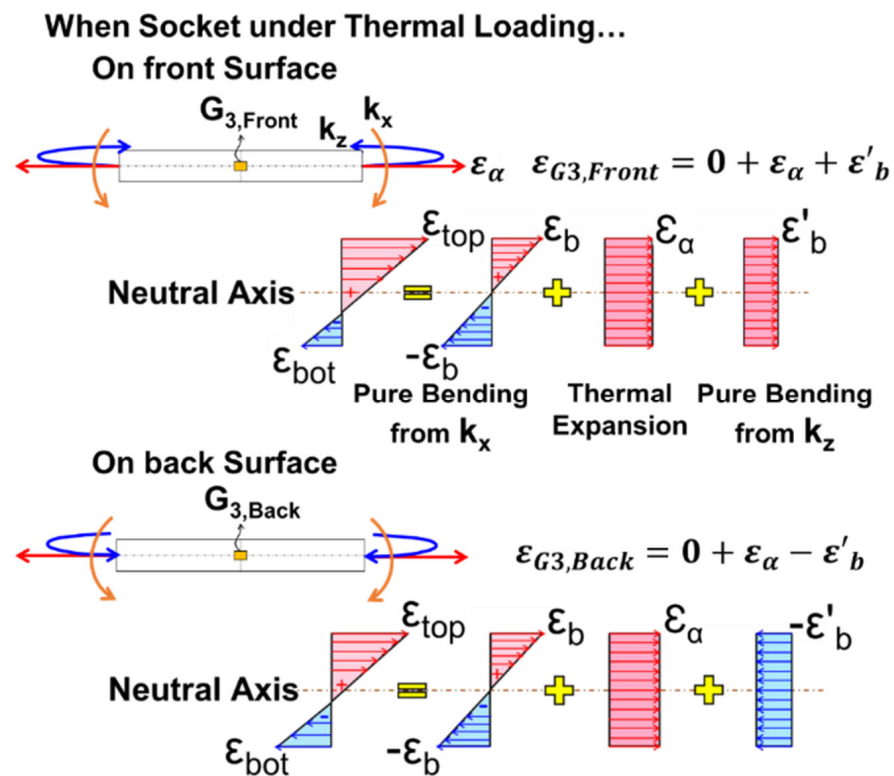


Figure 2. Strain distributions across the thickness of the DIMM socket under thermal loading.

If the strain gauge is attached on the front surface in the neutral axis, the strain ($\epsilon_{G3, Front}$) obtained from such gauge can be written as

$$\epsilon_{G3,Front} = 0 + \epsilon_{\alpha} + \epsilon'_{b} \quad (7)$$

Similarly, the strain ($\epsilon_{G3, Back}$) obtained from the back surface gauge is

$$\epsilon_{G3,Back} = 0 + \epsilon_{\alpha} - \epsilon'_{b} \quad (8)$$

The free thermal strain ϵ_{α} can be determined by

$$\epsilon_{\alpha} = \frac{\epsilon_{G3,Front} + \epsilon_{G3,Back}}{2} \quad (9)$$

Thus, the CTE (α) for the socket is obtained as

$$\alpha = \frac{\Delta\epsilon_{\alpha}}{\Delta T} \quad (10)$$

If ordinary strain gauges (not more expensive thermal gauges) are used in the CTE measurement of materials (such as the PCB and DIMM socket in this study), the temperature effect on gauge grid metal material and connected lead wire should be taken into account according to Equation (1). The approach used here was to adopt the concept of a compensation CTE (α_{comp}) by testing one known CTE material. A quartz (SiO_2) plate with $\alpha = 0.5 \text{ ppm}/^{\circ}\text{C}$ was tested using front and back strain gauges, shown in Figure 3. The average strain is plotted against the temperature. The line slope of average strain is the apparent CTE of $-5.72 \text{ ppm}/^{\circ}\text{C}$, but the CTE of quartz is actually $0.5 \text{ ppm}/^{\circ}\text{C}$. Therefore, the compensation CTE (α_{comp}) obtained from our gauge system is $6.22 \text{ ppm}/^{\circ}\text{C}$.

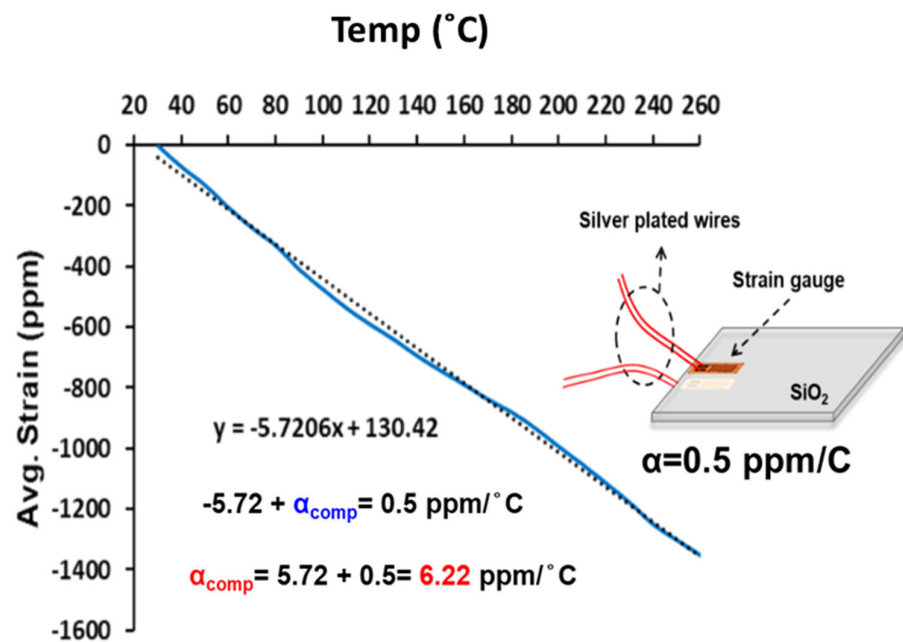


Figure 3. Calibration of strain gauge measurement for CTE measurement.

2.2. Shadow Moiré Measurements

Model PS600 provided by Akromatrix, one of the commercial shadow moiré systems, is shown in Figure 4a and was used in this study. The principle of the out-of-plane deformation measurement in the system is schematically shown in Figure 4b by illuminating the light through a mechanical grating on the surface of the specimen. The camera is for capturing the moiré fringe contours, while the movement of the stage driven by a servomotor is for phase shafting in order to enhance the spatial resolution of the measurement. This system features a spatial resolution of $2.5\mu\text{m}$ at a temperature range from 0 to 300°C , with a heating rate of 2°C/s and cooling rate of 1°C/s . Two kinds of test samples, the bare PCB and a socket-PCB assembly with 6 sockets, shown in Figure 5a,b, respectively, were tested in the moiré system by measuring the surfaces of their PCBs.

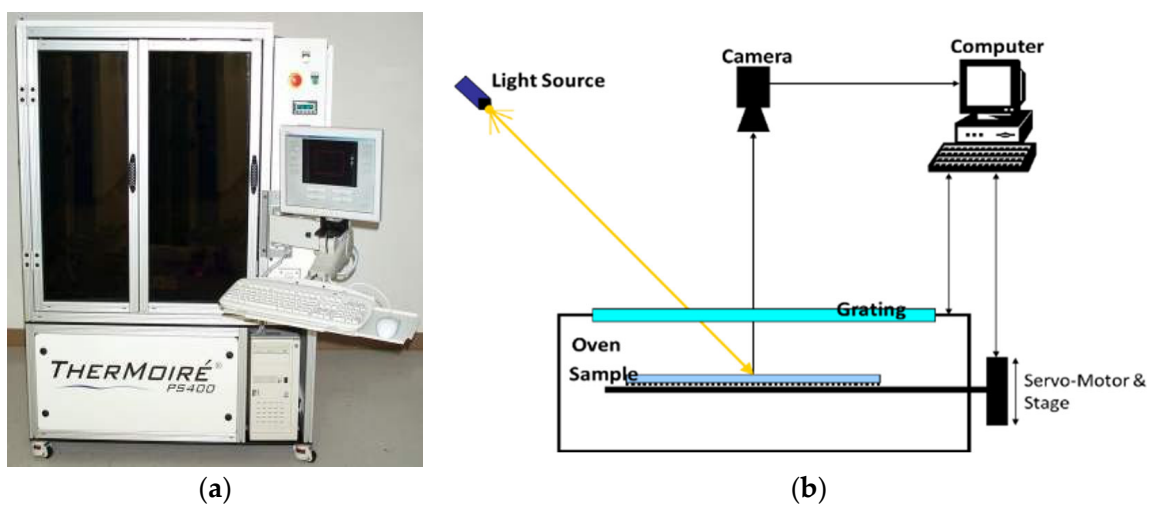


Figure 4. (a) Commercial shadow moiré system, and (b) schematic of the principle of out-of-plane deformation measurement in the system.

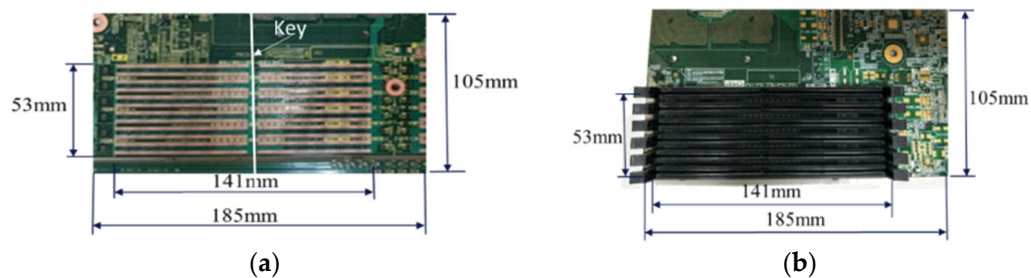


Figure 5. Configurations of the test specimens: (a) the bare PCB and (b) a socket-PCB assembly with 6 sockets (a local assembly).

2.3. Theoretical Analysis and FEM Simulation

For the theoretical analysis, a schematic of a quarter model of a socket-PCB assembly with one socket and its related geometric and material parameters are shown in Figure 6.

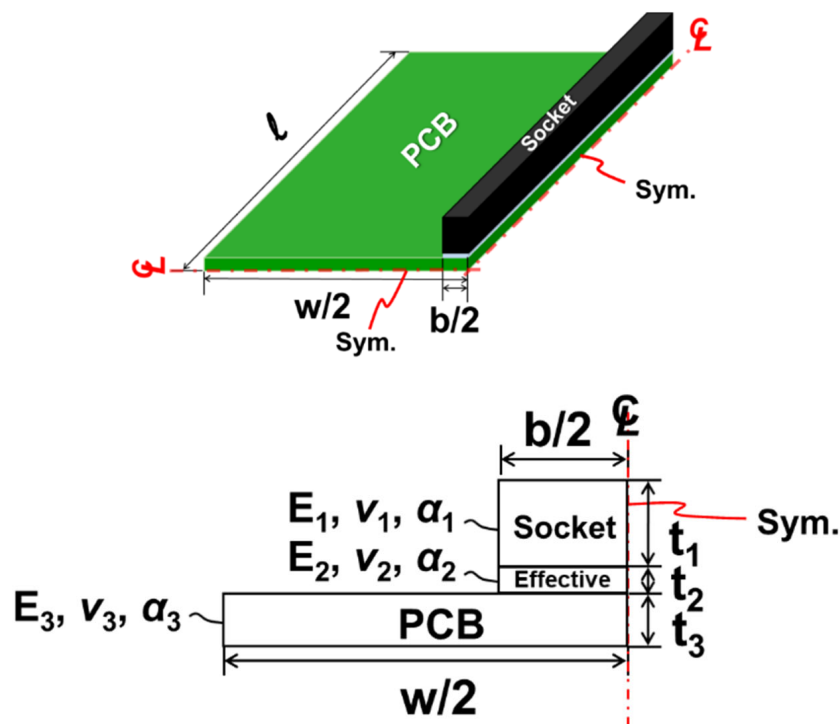


Figure 6. Quarter model of a socket-PCB assembly with one socket and its related geometric and material parameters in the theoretical formulation.

Based on the Suhir theory [13,14] and its modified version [15], the thermal deflection $w(x)$ of the socket-PCB assembly can be revised by considering the beam-like deformation and expressed as

$$w(x) = \frac{t\Delta\alpha\Delta T}{2\lambda D} \left[\frac{1}{2}x^2 - \frac{\cosh k_a x - 1}{k_a^2 \cosh k_a l} \right] \tag{11}$$

where $t = t_1 + t_2 + t_3$; $k_a = \sqrt{\frac{\lambda}{\kappa}}$; $\kappa = \frac{t_1}{3G_1 b} + \frac{2t_2}{3G_2 b} + \frac{t_3}{3G_3 W}$; $G_i = \frac{E_i}{2(1+\nu_i)}$; $\lambda = \frac{1}{E_1 t_1 b} + \frac{1}{E_3 t_3 W} + \frac{t^2}{4D}$; and $D = \frac{E_1 t_1^3 b}{12} + \frac{E_2 t_2^3 b}{12} + \frac{E_3 t_3^3 W}{12}$.

The thermal load is

$$\Delta T = T_f - T_i \tag{12}$$

where T_f is a final temperature and T_i is an initial one. The difference of thermal expansion coefficient ($\Delta\alpha$) between the socket (α_1) and the PCB (α_3) is

$$\Delta\alpha = \alpha_3 - \alpha_1 \quad (13)$$

The E , ν , α , and t denote the elastic modulus, Poisson's ratio, the thermal expansion coefficient, and the thickness of each layer, respectively, with subscripts from 1 to 3 representing the socket, effective adhesive, and PCB. The b and W are the width of the socket (or effective adhesive) and the PCB, respectively. The above-mentioned equations can be used for thermal warpage calculations of the one-socket-PCB assembly.

For the FEM simulation, a quarter model for the one-socket-PCB assembly is shown in Figure 7a with two planes of symmetry and a zoomed-in area. The zoomed-in area has two different geometries shown in Figure 7b: one with a full model (including socket housing, Cu pins, and solder joints) and the other with a simplified socket model (only including socket housing and effective material). Note that the simplified socket model used here is to prepare for analyzing more complicated structures of a multi-socket-PCB assembly. Material properties used in the theoretical analysis and FEM simulation are listed in Table 1, in which the α for the socket and PCB and the E for the socket were actually measured in this study, and the rest of them except for E_2 were provided by material vendors. The E_2 for the effective material of the pin solder joint is varied in the analyses and then approximated by the FEM simulation.

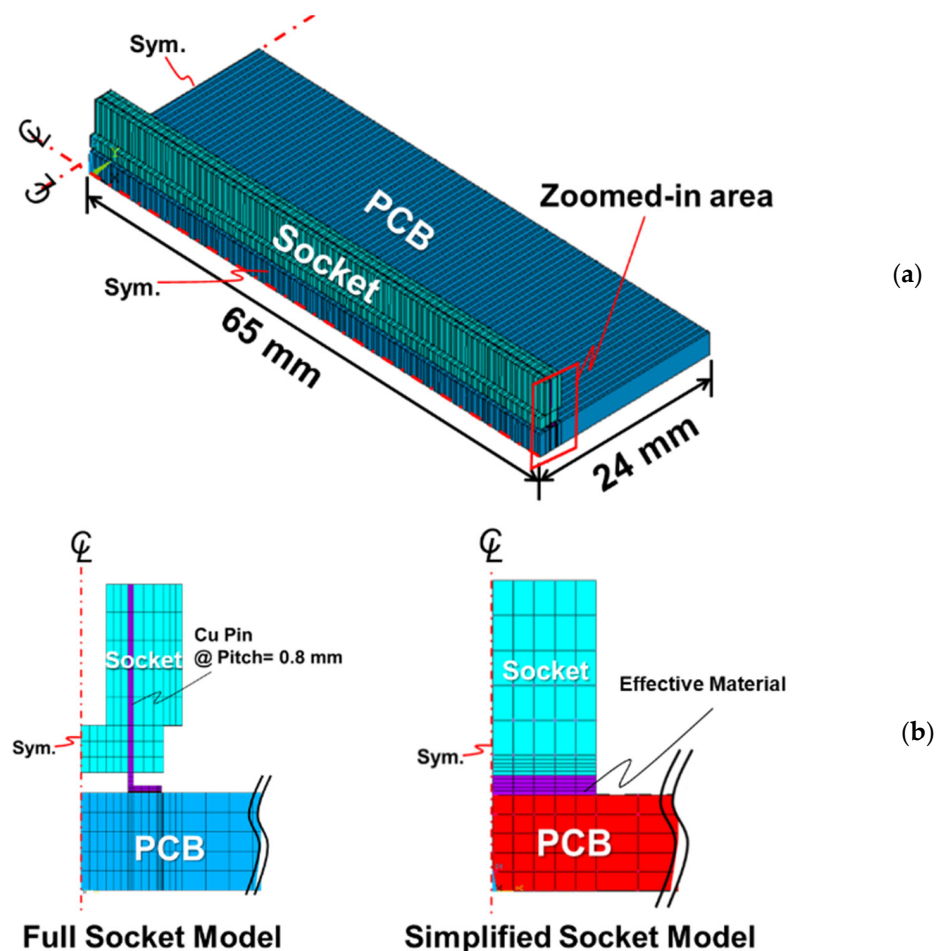


Figure 7. (a) A quarter FEM model for a one-socket-PCB assembly (b) with full and simplified socket models in the zoomed-in area.

Table 1. Material properties for the theoretical analysis and FEM simulation. (Note: The α for the socket and PCB and the E for the socket were measured in this study, while the rest of them except for E_2 were provided by material vendors.)

Material	E (GPa)	α (ppm/°C)	ν
Socket	8.7	14	0.3
Pin Solder Joint (Effective)	E_2	8.1	0.3
PCB	20	18	0.42
Cu Pin	120	16.9	0.3
Solder	30	22	0.3

3. Results and Discussion

The obtained results of the measurements and modelling for the thermally induced warpages of the DIMM socket-PCB assembly will be extensively discussed individually in this section, including material property measurements of the socket and the PCB, FEM modelling, thermal warpage measurements, warpage comparisons from different analyses, and warpages of the socket-PCB assembly after solder reflow.

3.1. Material Property Measurements

(a) Elastic Modulus and CTE of DIMM Socket

Since the DIMM socket is a hollow structure with many Cu pins inside, it is difficult to calculate or measure its elastic modulus. The effective elastic modulus was adopted and determined by performing the three-point bending test for the socket shown in Figure 8a, associated with the related FEM modelling of the test in Figure 8b, and then the effective elastic modulus can be determined as 8.7 GPa from the load–displacement curves obtained from the test and FEM simulation shown in Figure 8c. Furthermore, both bending strain distributions shown in Figure 8d across the thickness of the socket with and without Cu pins from the FEM simulation reveal that the neutral axis (with zero strain) is located at half of the socket thickness. This helps the CTE measurement of the socket using the strain gauge. Since the data of the CTE are more influential than those of the elastic moduli in terms of the thermal warpage according to Equation (11), the CTEs of the socket and PCB should be precisely determined later.

Moreover, typical strain data from the front and back gauges located at the neutral axis of a socket during the second, third, and fourth thermal loading cycles were obtained and are shown in Figure 9a. Note that the average of the front and back strains represents the thermal expansion strain, and the slope of the curve is the CTE, based on Equations (9) and (10). The obtained CTEs need to be added to α_{comp} (=6.22 ppm/°C) to exclude the thermal effect on the gauge and the connected wires. Then, the CTEs of three sockets (no. 1 to no. 3), obtained from gauges for these three thermal cycles, are shown in Figure 9b with their average of 14 ppm/°C. However, the strain data from the front and back gauges for those three sockets during the first thermal loading cycle are shown in Figure 10a, which are drastically dissimilar to those in Figure 9a, especially for temperatures beyond 120 °C. The CTE data extracted from the first thermal cycle are further shown in Figure 10b in comparison with those from the second to fourth cycles. The CTEs of three sockets are found to be not stable for the first thermal cycle, especially at temperatures higher than 120 °C, but stable after the first thermal cycle. Such variability in the CTEs may be attributed to the partially cured polymer of the socket before the first thermal cycle.

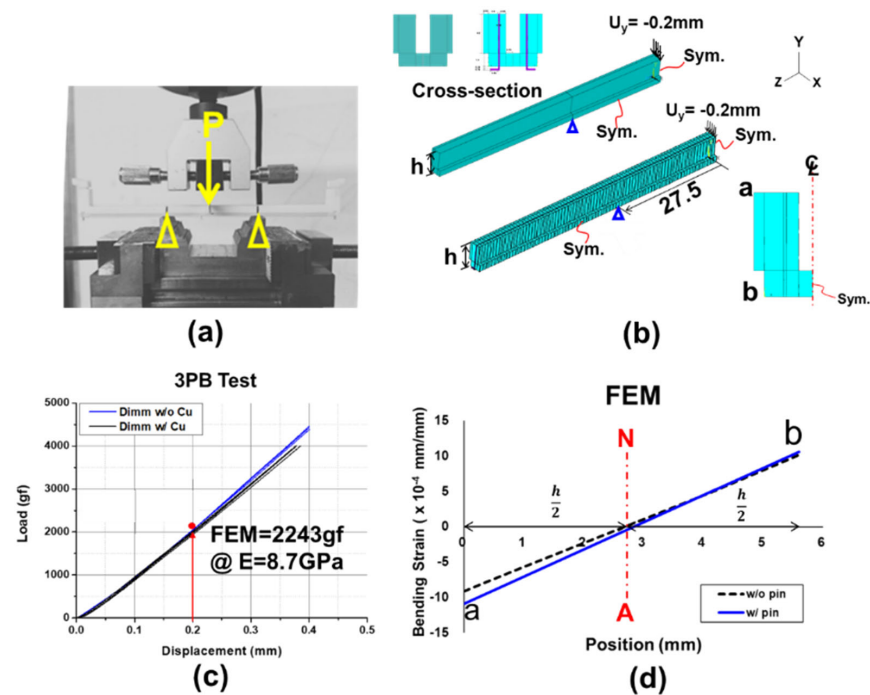


Figure 8. (a) Three-point bending test for a socket, (b) FEM modelling of the test, (c) determination of effective elastic modulus from load–displacement curves obtained by the test and FEM simulation, and (d) bending strain distributions across the thickness of the socket with and without Cu pins from the FEM simulation.

(b) CTE of Bare PCB

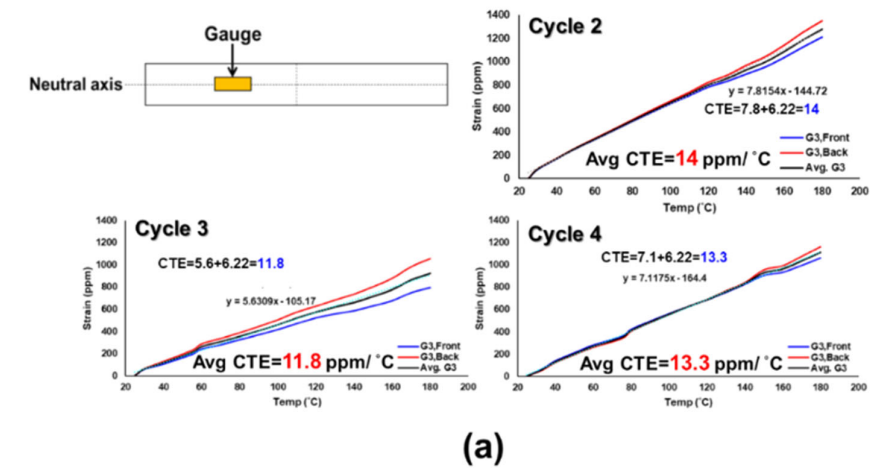
The strain gauges were also applied for the CTE measurement of the bare PCB. Typical strain data from three pairs of the front and back gauges (located at G_A , G_B , and G_C) on the PCB under thermal loading are shown in Figure 11a. The corresponding average strains are shown in Figure 11b for those three pairs of gauges during two thermal cycles and then the obtained average CTE of the bare PCB are about 18 ppm/°C. It is found that, unlike the socket, the CTE data of the bare PCB is much more stable and consistent during the thermal cycling.

3.2. FEM Modelling

(a) Model Validation and Comparison with Theory

To simplify the FEM calculation, the simplified socket model (shown in Figure 7b) was adopted in the simulation instead of the full socket model. The results of thermally induced warpages (at point a') for a one-socket-PCB assembly are shown in Figure 12a with various effective moduli (E_2) of the joint under different thermal loadings (ΔT). It is apparent that the warpage linearly depends on the thermal loading, but depends quite nonlinearly on the effective moduli of the joint. Meanwhile, for replacing the full socket model with the simplified one, the acceptable E_2 should be determined and used for the FEM simulation afterward. For this, the thermal warpage obtained from the full socket model is also plotted in Figure 12a in comparison with those from the simplified one. It can be seen that the simplified socket model with $E_2 = 100$ MPa can be representative of the full one with the same warpage values. Moreover, a further comparison of the out-of-plane deformations (along the line a-a') of the one-socket-PCB assembly under thermal loading $\Delta T = 150$ °C with $E_2 = 100$ MPa is shown in Figure 12b from the FEM simulations with full and simplified socket models. The consistency of both models is ensured again. Therefore, it is feasible to apply the simplified socket model associated with $E_2 = 100$ MPa to the rest of the FEM simulations in this study. The theoretical result of the deformation is also plotted in Figure 12b, compared with the FEM ones. It is seen that the theoretical solution, with slight

overprediction, is consistent with both FEM results. For further parametric study, the effect of the width of the PCB on the thermal warpage of a one-socket-PCB assembly along the socket line is shown in Figure 13a from the theoretical and FEM analyses for $E_2 = 100$ MPa and 1000 MPa. Both results indicate that the thermal warpage decreases with increasing the width of the PCB, and the discrepancy between both results is relatively lower for $E_2 = 1000$ MPa. Furthermore, the effects of effective modulus E_2 and thickness t_2 are also demonstrated in Figure 13b from both analyses with $W/b = 7.5$ under $\Delta T = 150$ °C. It can be seen that the thermal warpage decreases with increasing the thickness t_2 but decreasing the effective modulus E_2 . However, both parametric effects become relatively insignificant as the effective modulus E_2 is larger than 1000 MPa. It is noted from Figures 12 and 13 that a slight overprediction of the theoretical solution in comparison with the FEM one, especially for a low effective modulus E_2 , is also found in the literature [16] due to the limitation of the plate or beam assumption used in the theoretical formulations. Although our concern in this study is mainly with the warpage of the assembly, interfacial stresses are also important and comprehensively discussed [17] in the joint of the assembly.



(b)

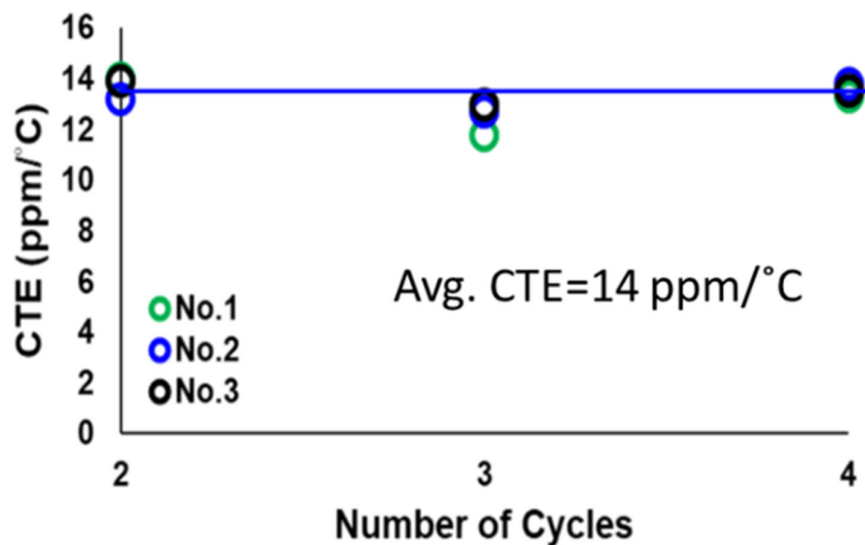


Figure 9. (a) Typical strain data from the front and back gauges located at the neutral axis of a socket during the second, third, and fourth thermal cycling loading, and (b) the CTEs of three sockets, obtained from gauges for these three thermal cycles.

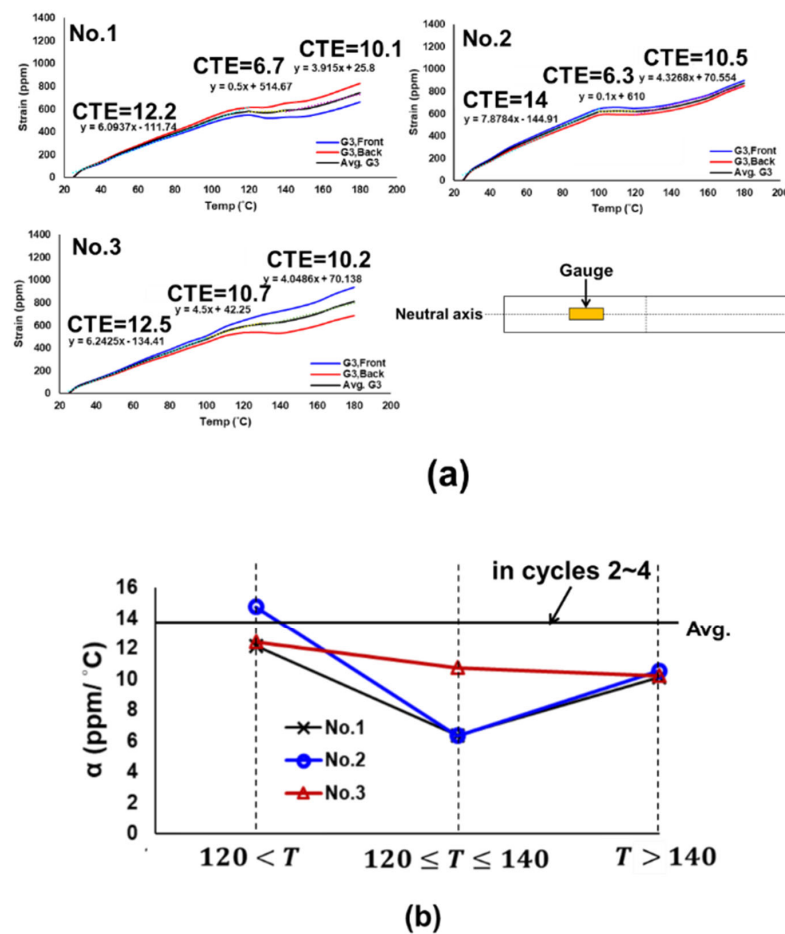


Figure 10. (a) Strain data from the front and back gauges for three sockets during the first thermal loading cycle, and (b) temperature-dependent CTEs of three sockets obtained from gauges for the first thermal cycle and their comparison with those for the second to fourth cycles.

(b) Local Model vs. Full Model

Since the test specimen is cut from the full socket-PCB assembly, the local model representing the test specimen has to be ensured to have the same behavior as the full model. Both local and full models under thermal loading $\Delta T = 150$ °C were analyzed by the FEM simulation. The results of the out-of-plane deformations along the socket line o-a and their contour maps for the socket-PCB assembly are shown in Figure 14. It is obvious that, even though both contour maps look quite different due to different settings of the zero-deformation positions, the out-of-plane deformations along the socket line for both models are almost identical. Therefore, investigating the test specimen by experimental and FEM analyses can help in understanding the thermal deformation behavior of the full socket-PCB assembly.

3.3. Thermal Warpage Measurement

(a) Bare PCB

The out-of-plane deformation contours of the bare PCB from the moiré measurement at various temperature are shown in Figure 15a, and the out-of-plane deformations of the bare PCB along three socket lines (A, B, and C) in which the sockets will be located are plotted in Figure 15b. Note that the positive value of the deformation is concave, while the negative value indicates convex. The key line is a line with six through vias for fixing the socket on the PCB before the solder reflow. It is shown that the bare PCB at room temperature ($T = 30$ °C) is slightly concave and becomes flatter after heating up. The thermally induced deformations of two bare PCB specimens along those three lines at

various temperature loadings (ΔT) are shown in Figure 16a, which were extracted from the moiré data. The corresponding warpages of the two bare PCB specimens along the socket lines at various thermal loadings are shown in Figure 16b. The results indicate that the bare PCB subject to the thermal heat loading deforms convex with a socket line warpage value between $-5 \mu\text{m}$ and $-25 \mu\text{m}$ at $\Delta T = 150 \text{ }^\circ\text{C}$.

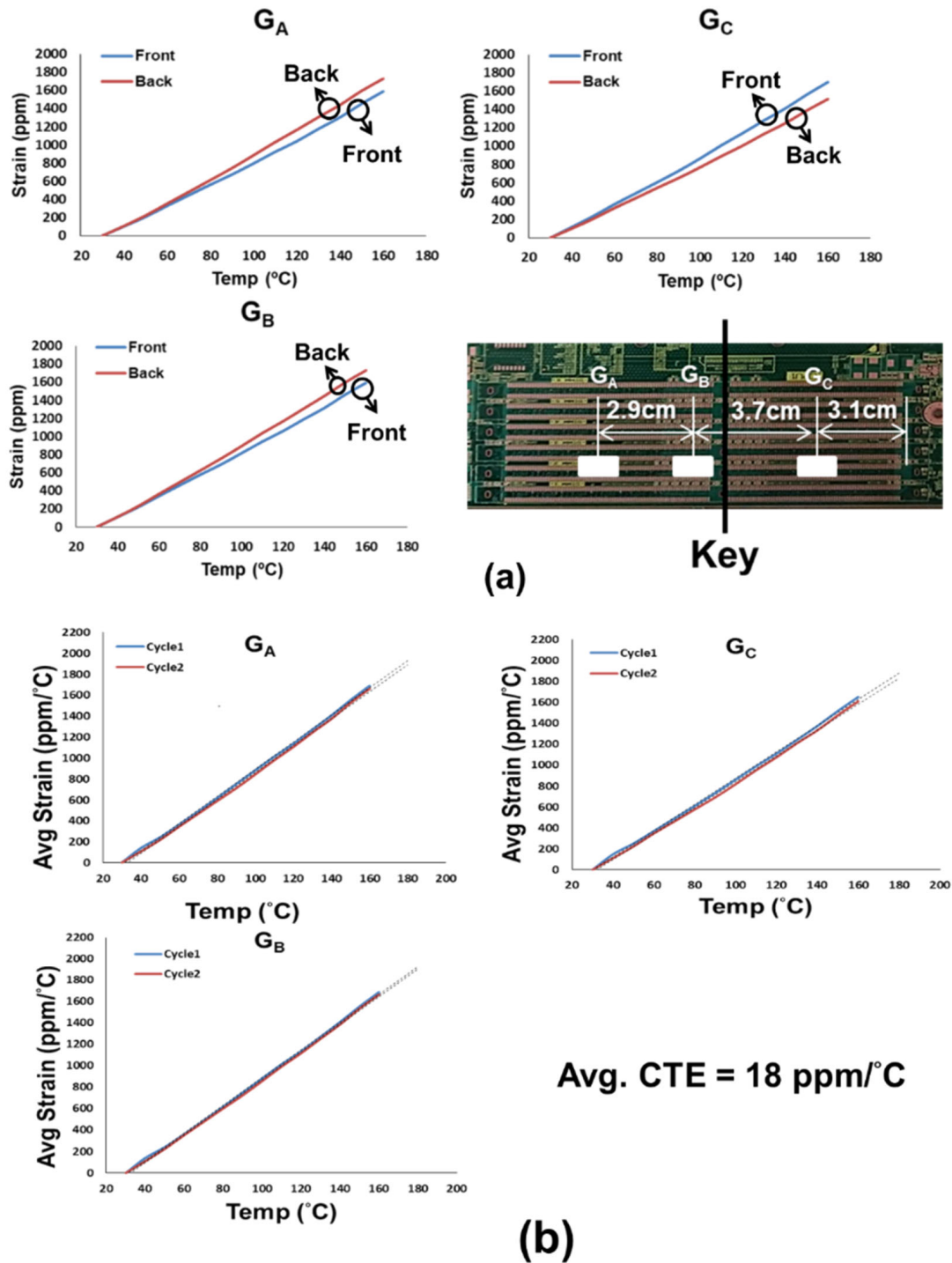


Figure 11. (a) Typical strain data from three pairs of front and back gauges (G_A , G_B , and G_C) on the bare PCB under thermal loading, and (b) average strains from front and back gauges for those three pairs during two thermal cycles and the CTEs of the PCB obtained from those average strain data.

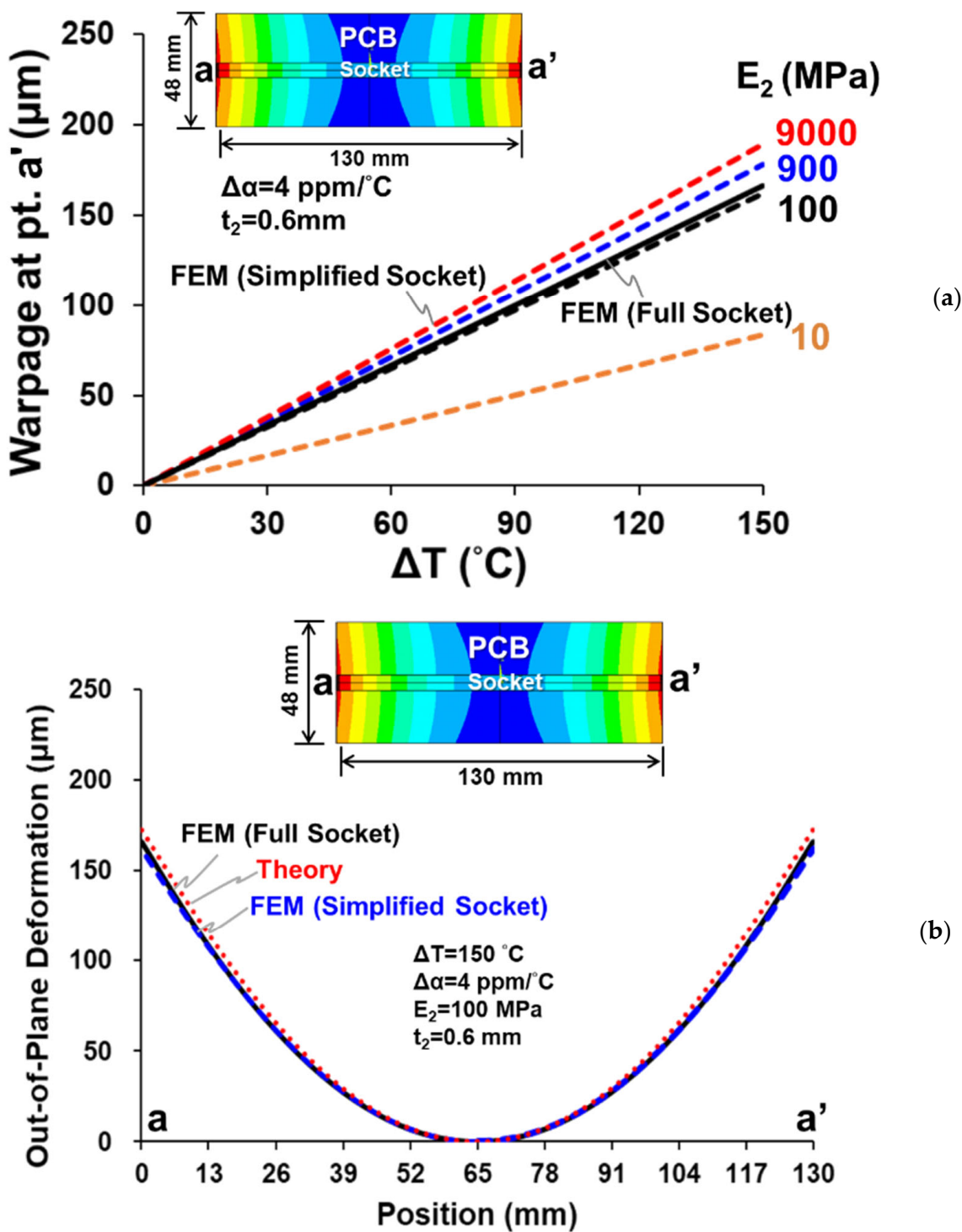
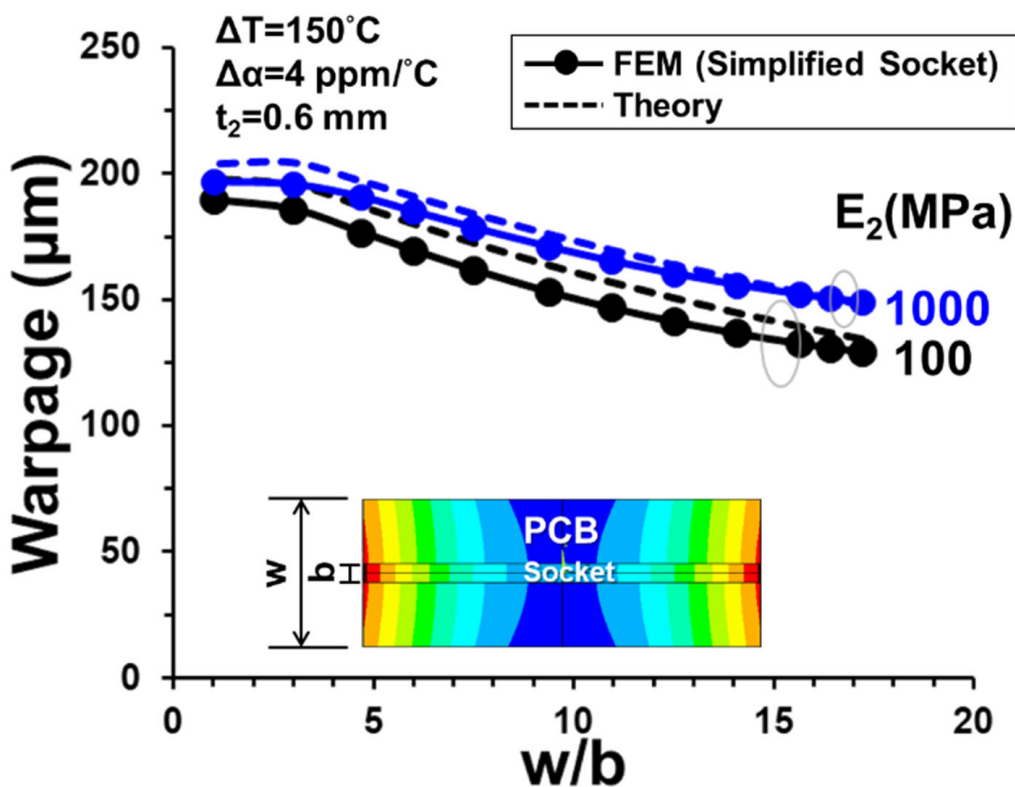
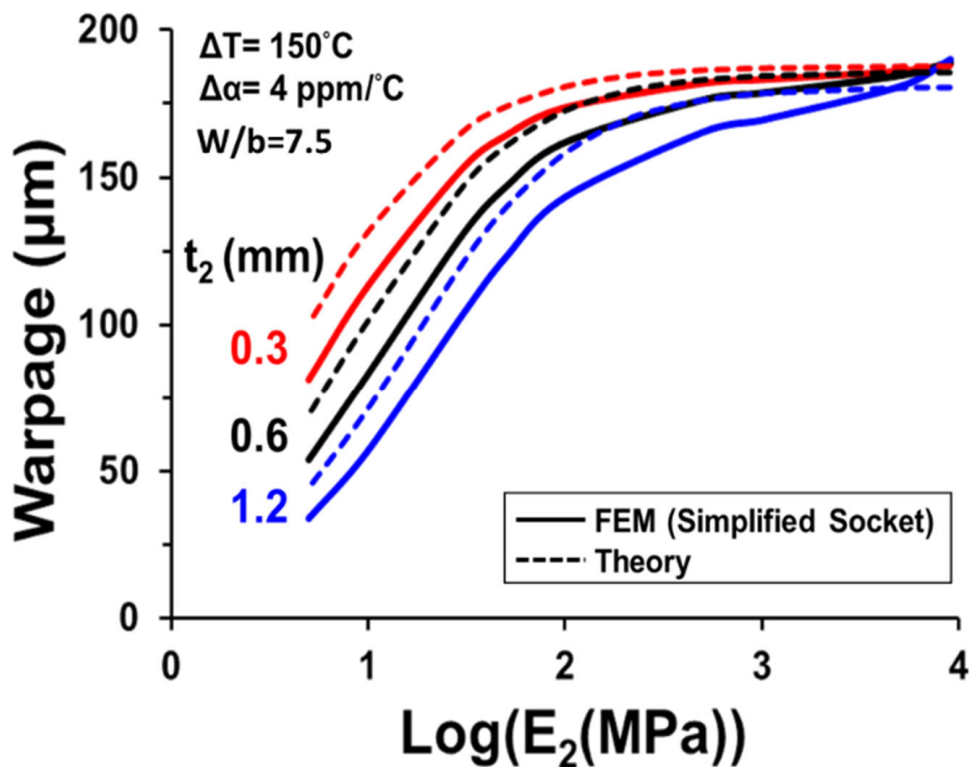


Figure 12. (a) Thermally induced warpage (plus an inset of full-field deformation contours) of a one-socket-PCB assembly with various effective moduli of the joint under different thermal loadings (ΔT) from FEM with full and simplified socket models, and (b) the out-of-plane deformations (along the line a-a') of the one-socket-PCB assembly under thermal loading $\Delta T = 150\text{ }^\circ\text{C}$, from the theory and FEM simulations with full and simplified socket models.



(a)



(b)

Figure 13. Thermally induced warpage of a one-socket-PCB assembly (a) with various widths of the PCB for $E_2 = 100 \text{ MPa}$ and 1000 MPa , and (b) with various E_2 and t_2 but $W/b = 7.5$ under $\Delta T = 150 \text{ }^\circ\text{C}$ from the FEM with simplified socket model and the theory.

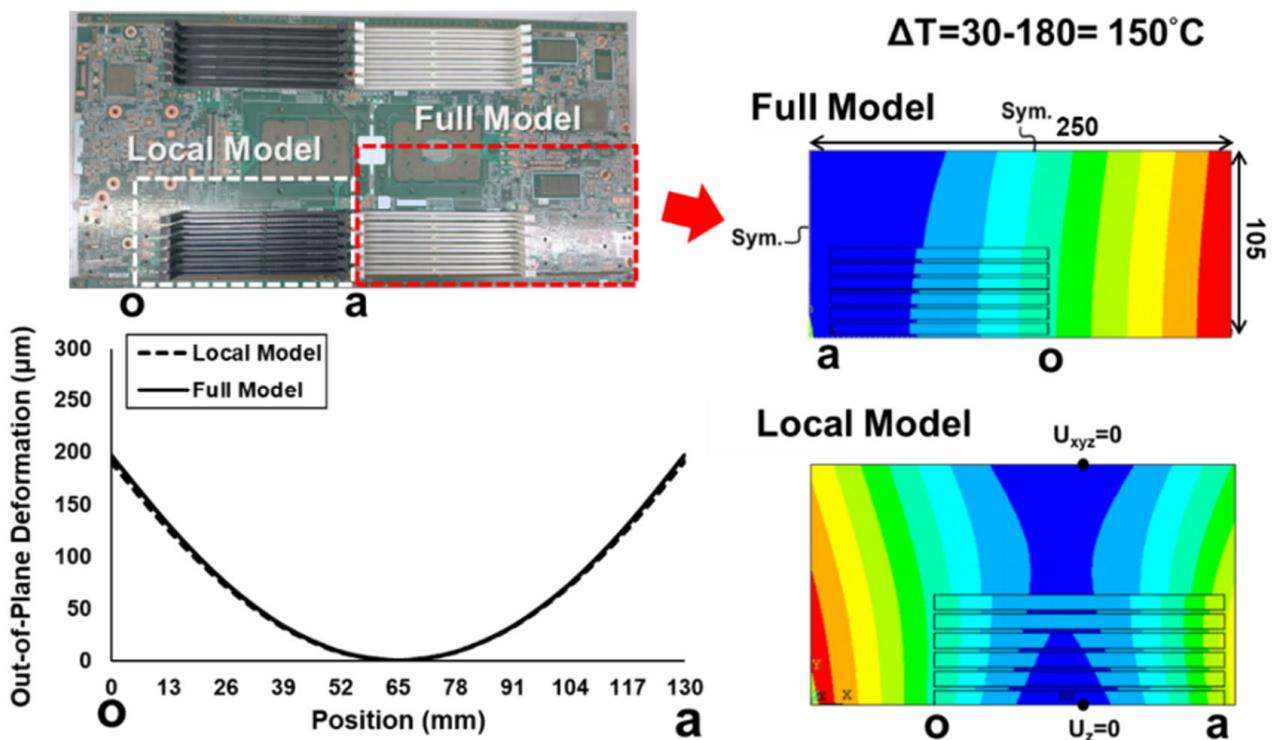


Figure 14. The out-of-plane deformations along the socket line o-a and their contour maps for the socket-PCB assembly under thermal loading $\Delta T = 150^\circ\text{C}$, determined from the FEM simulation using a local model and a full model.

(b) Socket-PCB Assembly

The out-of-plane deformation contours of the six-socket-PCB assembly, obtained from moiré measurements at various temperatures, are shown Figure 17a and their out-of-plane deformations of this assembly along the socket lines (A to C) are also plotted in Figure 17b with setting zero deformation at the key line. It can be seen that the concave-shape deformation increases with an increase in temperature. Furthermore, by subtracting the deformation at 30°C , thermally induced deformations for two samples of the six-socket-PCB assembly along the socket lines at various temperature loadings (ΔT), obtained from moiré measurements, are shown in Figure 18a, and the corresponding warpages of those two samples along the socket lines at various temperature loadings (ΔT) are presented in Figure 18b. Those results indicate that the thermally induced warpage along the socket lines increases linearly with temperature loading and its variation is less significant between the different socket lines as well as between the samples.

3.4. Comparisons of Thermal Warpages from Moiré, Gauges, Theory, and FEM

The thermally induced deformations of the six-socket-PCB assembly along the socket lines (line o-a) at various temperature loadings (ΔT) are shown in Figure 19a from moiré measurements, theory, and FEM simulation, and in Figure 19b for their corresponding warpages along the socket lines at various temperature loadings (ΔT). Note that moiré data presented here have been modified by considering the thermal warpage of the bare PCB observed in Figure 16b, while the $b = 6 \times 6.4\text{ mm} = 38.4\text{ mm}$ and $W = 105\text{ mm}$ were used in the theoretical analysis. It is found that all moiré, theoretical, and FEM results are reasonably consistent, either for thermally induced deformations or warpage along the socket lines. Moreover, the front and back gauges located at the PCB near the middle of the socket lines on the socket-PCB assembly were used for measuring the bending strains (or curvature) under two thermal loading cycles. The obtained data are shown in Figure 20a for the apparent strains from the front and back gauges under two thermal

cycles. Additionally, the gauge-determined corresponding warpage along the socket line is obtained and shown in Figure 20b by converting those strains to bending strain, curvature, and warpage data using Equations (4)–(6), respectively. It is found that the thermally induced warpage along the socket line, measured by the gauges, increases linearly with temperature at the beginning, but starts dropping near $T = 180\text{ }^{\circ}\text{C}$. This turning-around mechanism cannot be clearly understood at this moment but could be discussed later. It is also shown that the gauge results are in good agreement with the moiré data, especially for those along the socket line A.

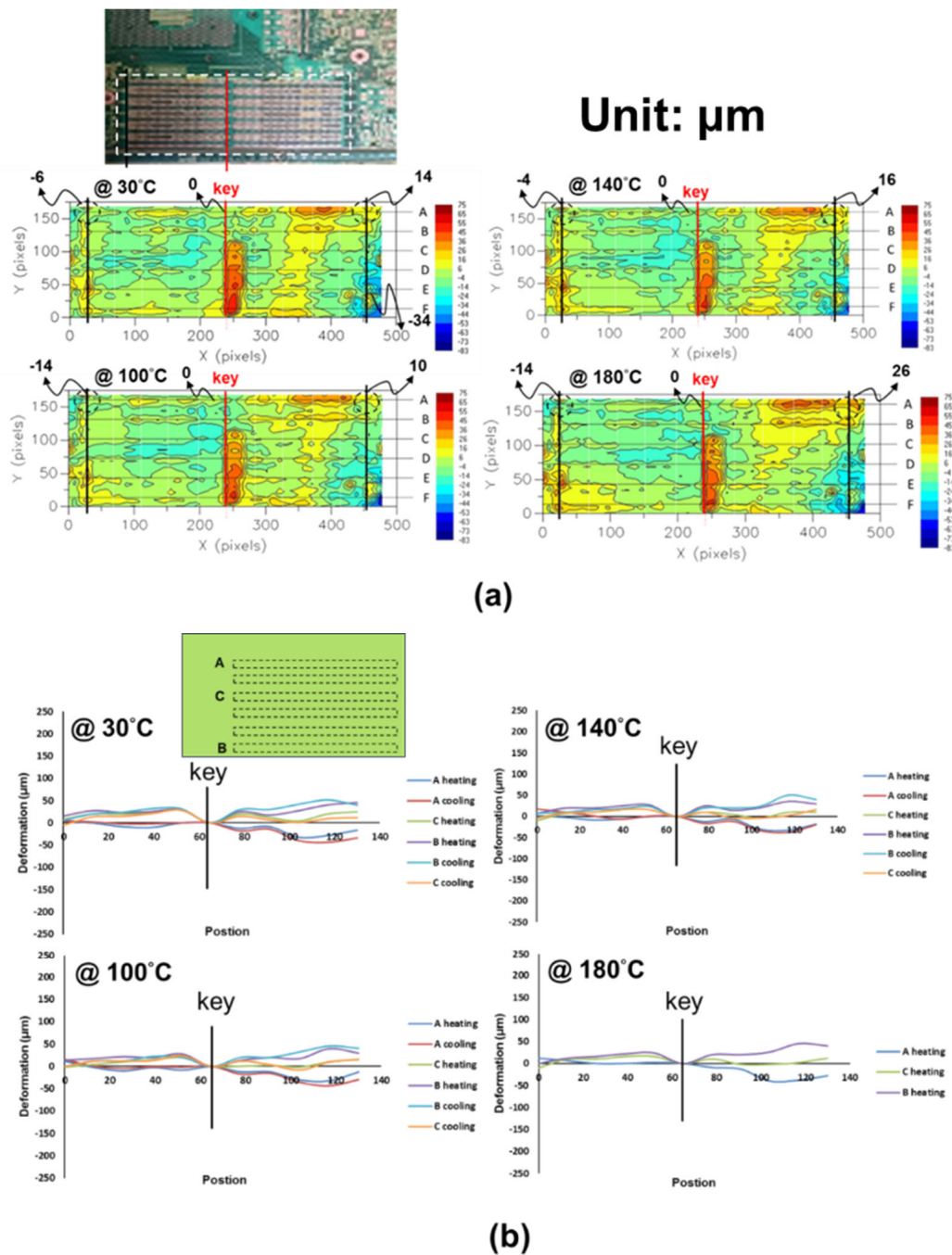


Figure 15. (a) Out-of-plane deformation contours (in dotted line box) for the bare PCB at various temperatures, obtained from moiré measurements, and (b) out-of-plane deformations of the bare PCB along three lines (A, B, and C) in which the sockets will be located.

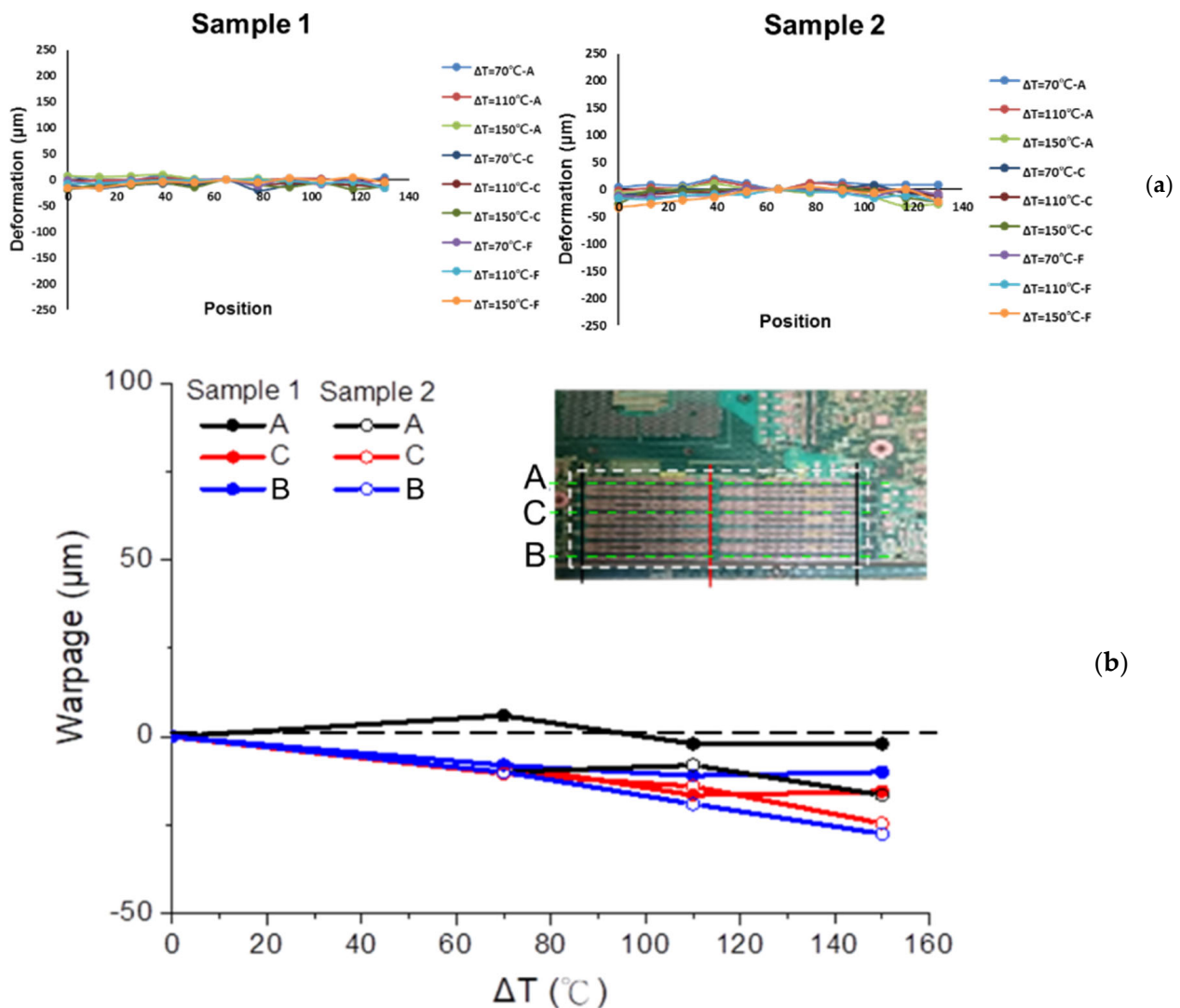


Figure 16. (a) Thermally induced deformations of two bare PCB specimens along the socket lines at various temperature loadings, obtained from moiré measurements, and (b) the corresponding warpages of the two bare PCB specimens along the socket lines (A, B, and C) at various temperature loadings.

3.5. Warpage of Socket-PCB Assembly after Solder Reflow

The cooling-rate effect on thermally induced warpages of the six-socket-PCB assembly after solder reflow was also studied. The gauge results of the warpage along the socket lines with two cooling cycles each at two different cooling rates ($0.6^\circ\text{C}/\text{min}$ and $1.2^\circ\text{C}/\text{min}$, corresponding, respectively, to 6 h and 3 h of cooling time from 250°C to 30°C) are shown in Figure 21, compared with those from the theory and FEM simulation. Note that the negative value of the warpage indicates the concave-down deformation. It is found that the zero thermal warpages are maintained down to 180°C from 250°C during the cooling, and those warpages have lower values with lower cooling rates, but the theoretical and FEM values give an upper bound for those. The reason behind it is that the lead-free solder (with a melting temperature of 217°C) used here is soft with a strong creep (visco-plastic) behavior at high temperatures and it could not generate a constraint between the socket and PCB until the temperature reached 180°C . Such a behavior has also been observed in a PBGA package-PCB assembly [11]. Additionally, the cooling-rate dependency of the thermal warpage is caused by the creep behavior of the solder joint. However, since the fast cooling rate of around $60^\circ\text{C}/\text{min}$ is generally adopted in the reflow process, the FEM

simulation without considering the creep behavior might give a good prediction of the thermal warpage of the socket-PCB assembly after the solder reflow. From the present observation of the zero warpage induced beyond 180 °C, it might indicate there is no constraint between the socket and PCB due to the very soft material property and high creep rate of the solder joints. That could be a reason for the warpage drop in the strain gauge data beyond 180 °C, as observed in Figure 20b.

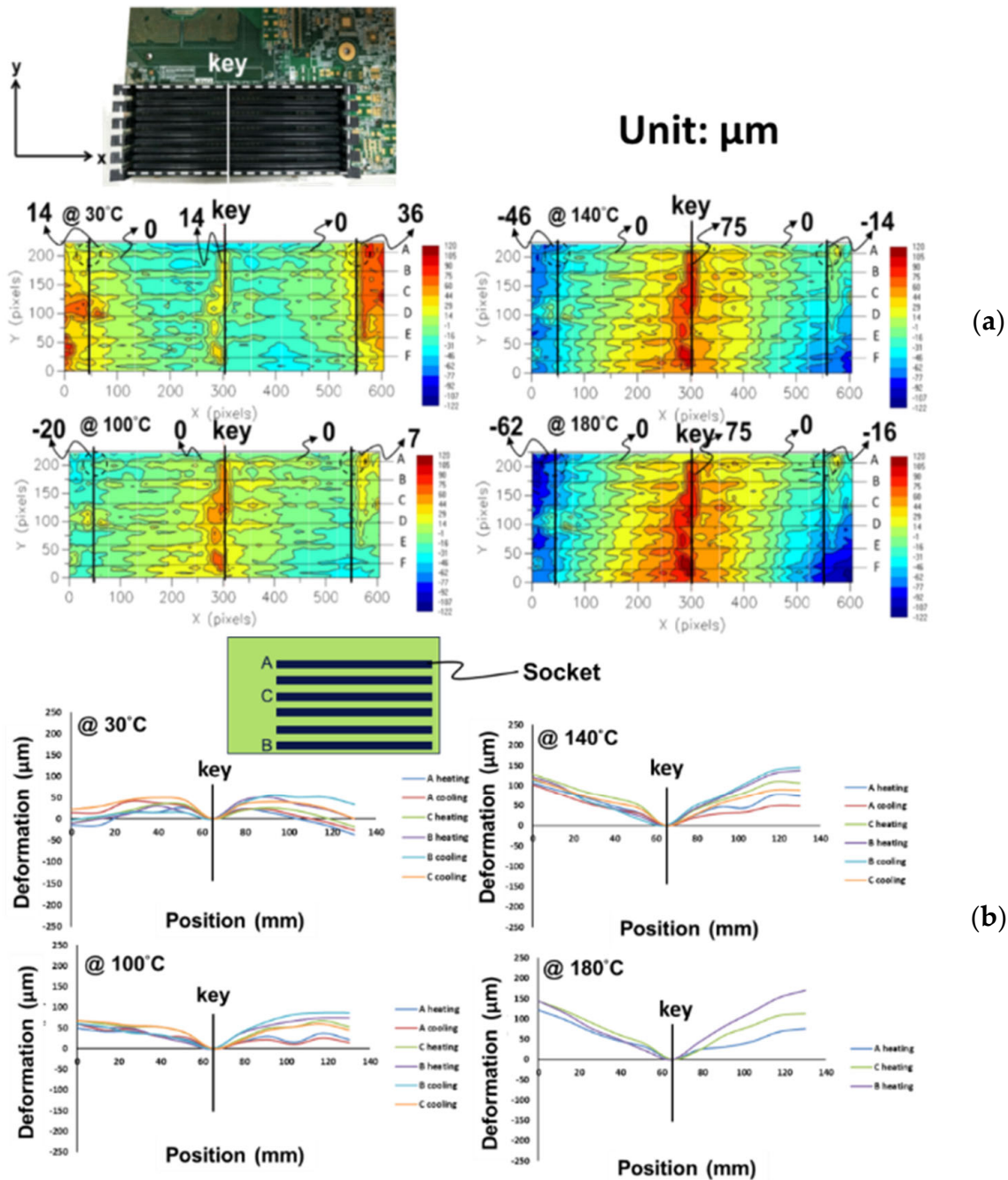


Figure 17. (a) Out-of-plane deformation contours (in dotted line box) for the six-socket-PCB assembly at various temperatures, obtained from moiré measurements, and (b) out-of-plane deformations of the socket-PCB assembly along the lines in which the sockets are located.

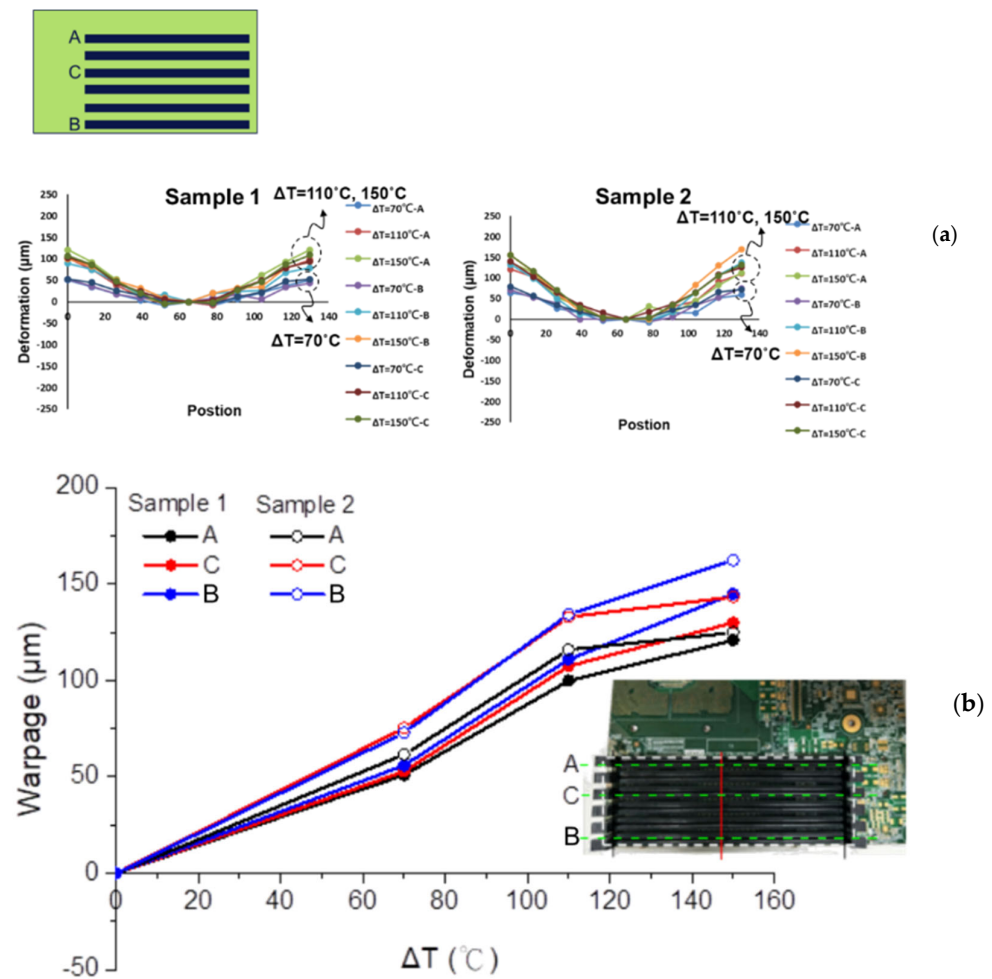


Figure 18. (a) Thermally induced deformations for two samples of the six-socket-PCB assembly along the socket lines at various temperature loadings (ΔT), obtained from moiré measurements, and (b) the corresponding warpages of the two samples along the socket lines at various temperature loadings (ΔT).

Based on the zero warpage occurring at the temperature of $180\text{ }^{\circ}\text{C}$, the effects of the thickness of the PCB (t_{PCB}) and mismatch of CTE ($\Delta\alpha$) between the socket and PCB on the thermally induced warpages of the PCB specimen with six sockets along the socket line (line o-a) and in the full field (in inserted graph) are shown in Figure 22 from the FEM simulation for thermal loading $\Delta T = 30\text{ }^{\circ}\text{C} - 180\text{ }^{\circ}\text{C} = -150\text{ }^{\circ}\text{C}$. The warpage data can represent those of the specimen cooling down after the reflow process. The thicknesses of the PCB here are taken based on the possible values in the application. The results indicate that the thermal warpage is linearly dependent on the $\Delta\alpha$, but nonlinearly dependent on the t_{PCB} . The linear dependence on the $\Delta\alpha$ and the nonlinear dependence on t_{PCB} can also be observed in Equation (11) for the thermal deflection from the theoretical solution. Moreover, the effects of both parameters are also applied to the specimen with 24 sockets on the PCB (like the configuration in Figure 1b). The results of the thermal warpage at the corner of the PCB (or the maximum warpage) and the full-field deformation are shown in Figure 23 with various t_{PCB} and $\Delta\alpha$ from the FEM simulation after solder reflow. It can be seen that, after the solder reflow, the socket-PCB assembly deforms cylindrically with a maximum warpage at the corner of the PCB and the maximum thermal warpage also depends linearly on the $\Delta\alpha$ and nonlinearly on the t_{PCB} . It is specially noted that the FEM results shown in Figures 22 and 23 were obtained by assuming that the bare PCB is always flat during the solder reflow heating and cooling process.

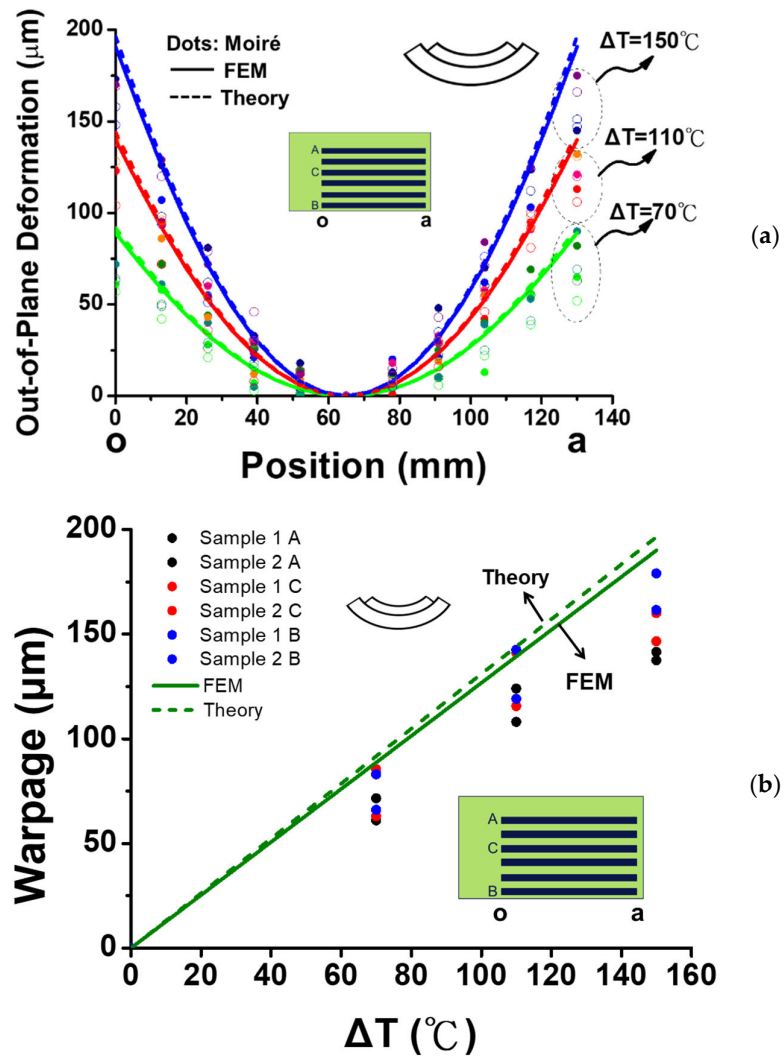


Figure 19. (a) Comparison of thermally induced deformations of the six-socket-PCB assembly along the socket lines (line o-a) at various temperature loadings (ΔT), obtained from moiré measurements, theory, and FEM simulations, and (b) the corresponding warpage comparison of the six-socket-PCB assembly along the socket lines at various temperature loadings (ΔT).

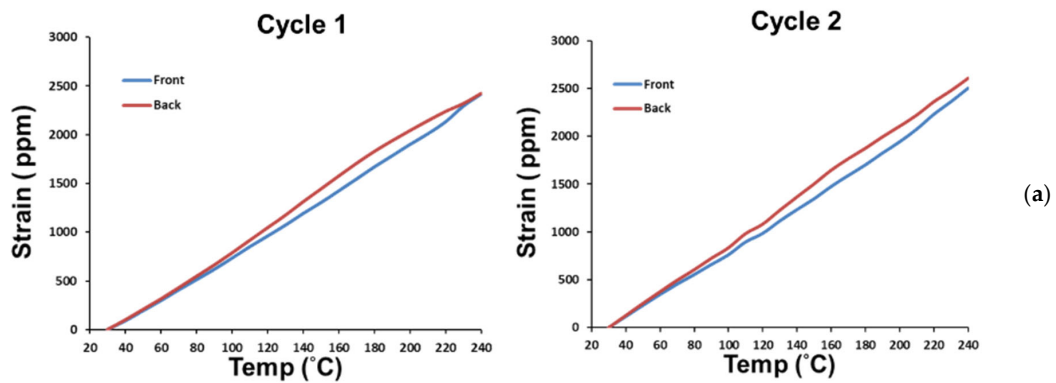


Figure 20. Cont.

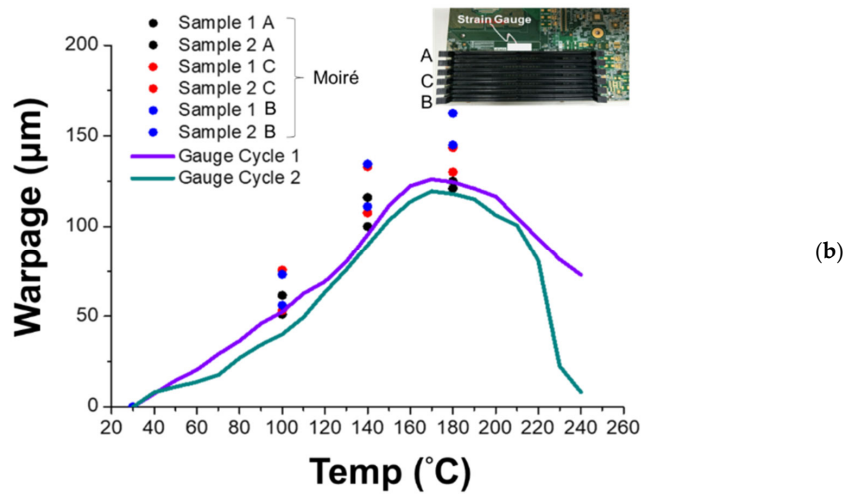


Figure 20. (a) Strain data of the front and back gauges on the six-socket-PCB assembly under two thermal loading cycles, and (b) the gauge-determined corresponding warpages of the six-socket-PCB assembly along the socket lines, compared with moiré results.

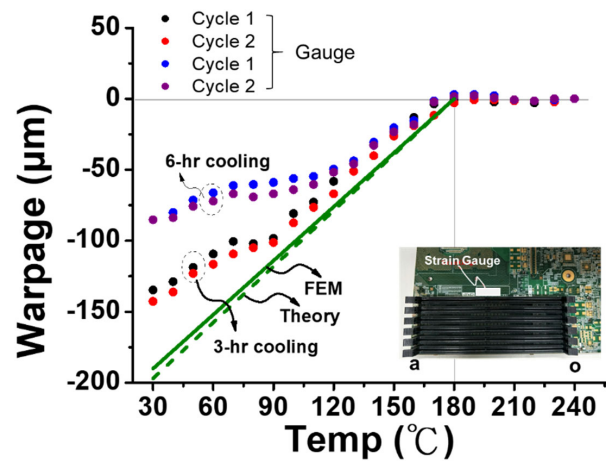


Figure 21. The cooling rate effect on thermally induced warpages of the six-socket-PCB assembly along the socket lines after solder reflow, from strain gauge, theory, and FEM simulation.

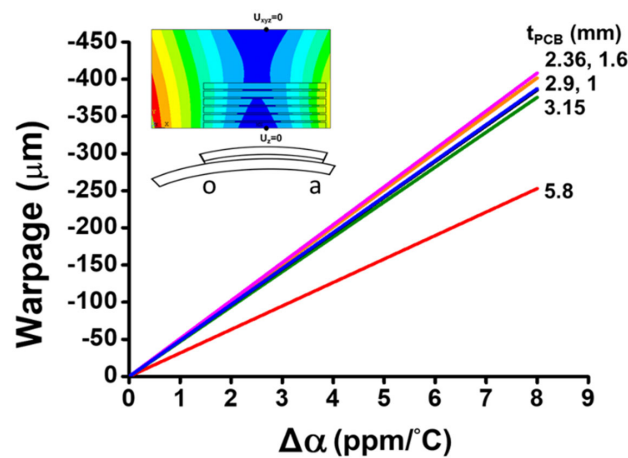


Figure 22. The effects of the thickness of the PCB (t_{PCB}) and mismatch of CTE ($\Delta\alpha$) on thermally induced warpages of the PCB specimen with six sockets along the socket lines (line o-a) from the FEM simulation for $\Delta T = 30\text{ }^{\circ}\text{C} - 180\text{ }^{\circ}\text{C} = -150\text{ }^{\circ}\text{C}$.

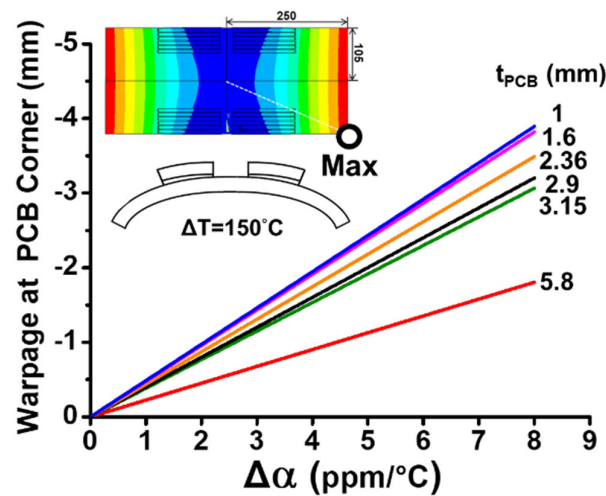


Figure 23. The effects of the thickness of the PCB (t_{PCB}) and mismatch of CTE ($\Delta\alpha$) on thermally induced warpages at the corner of the PCB for the socket-PCB assembly with 24 sockets from the FEM simulation $\Delta T = 30\text{ }^{\circ}\text{C} - 180\text{ }^{\circ}\text{C} = -150\text{ }^{\circ}\text{C}$.

4. Conclusions

The problem of thermal warpage for the DIMM socket-PCB assembly after the solder reflow processes has been extensively investigated experimentally, theoretically, and numerically, especially along the socket lines and over the entire assembly. In this study, a beam-like theoretical solution to this problem has been newly proposed by modifying the existing Suhir theory. The theoretical solution validated by the finite element method (FEM) simulation has provided the detailed mechanics, including the critical parameters, such as the coefficient of thermal expansion (CTE, α), elastic modulus (E_2), thickness (t_2) of the effective material (which is a combined material of a solder joint and Cu pin), and width of the PCB. The CTEs of the socket and the bare PCB have been obtained as 14 and 18 ppm/ $^{\circ}\text{C}$ by the strain gauge measurement, respectively. However, inconsistent data for the CTE were found for the sockets in the measurement of the first thermal cycle, but the CTE became constant after the first thermal cycle. Meanwhile, the effective elastic moduli of the socket and the combined material of solder joint and Cu pin have been determined by a hybrid method (combined with the experiment and FEM) and FEM simulations with a simplified model, respectively. Furthermore, the cylindrical-like thermal deformation and warpage of the bare and socket-PCB have been measured by the moiré experiment, and the thermally induced warpages of the socket-PCB assembly are also consistent with those from the theory and FEM simulations. Moreover, the result from the moiré-consistency strain gauge measurement for the thermal warpage of the socket-PCB assembly has revealed that the thermal warpage starts at 180 $^{\circ}\text{C}$ during the process of cooling down from the reflow peak temperature (250 $^{\circ}\text{C}$) and is dependent on the cooling rate due to the nature of the high creep (visco-plastic) behavior of the solder material. Finally, the thermally induced warpages of the full socket-PCB assemblies along the socket lines and over the entire assembly after the solder reflow process have been provided in this study by the validated FEM simulation in terms of the PCB thickness (t_{PCB}) and the CTE mismatch ($\Delta\alpha$) between the socket and PCB for future design and verification.

Author Contributions: Conceptualization, M.-Y.T., T.-M.L. and S.-T.C.; methodology, M.-Y.T., Y.-W.W. and Y.-J.L.; software, Y.-W.W. and Y.-J.L.; validation, M.-Y.T., Y.-W.W. and Y.-J.L.; formal analysis, Y.-W.W. and Y.-J.L.; investigation, Y.-W.W. and Y.-J.L.; resources, M.-Y.T., T.-M.L. and S.-T.C.; data curation, Y.-W.W. and Y.-J.L.; writing—original draft preparation, M.-Y.T. and T.-M.L.; writing—review and editing, M.-Y.T. and T.-M.L.; visualization, M.-Y.T. and T.-M.L.; supervision, M.-Y.T.; project administration, T.-M.L. and S.-T.C.; funding acquisition, M.-Y.T., T.-M.L. and S.-T.C. All authors have read and agreed to the published version of the manuscript.

Funding: This study was supported by the Ministry of Science and Technology (MOST), Taiwan and Inventec Corporation under projects No. MOST-111-2221-E-182-045 and SCRPD2H0391, respectively.

Institutional Review Board Statement: Not applicable.

Informed Consent Statement: Not applicable.

Data Availability Statement: On inquiry, the data presented in this study is available from the authors.

Conflicts of Interest: The authors declare no conflict of interest.

References

1. Lau, J.H. Recent advances and trends in advanced packaging. *IEEE Trans. Compon. Packag. Manuf. Technol.* **2022**, *12*, 228–252. [[CrossRef](#)]
2. Dally, J.W.; Riley, W.F. *Experimental Stress Analysis*, 14th ed.; College House Enterprises: Knoxville, TX, USA, 2006.
3. Mercado, L.L.; Hsieh, G.; Girouard, S. Electronic packaging solder joint reliability assessment with a mechanics-based strain gauge methodology. *IEEE Trans. Packag. Technol.* **2006**, *29*, 5–12. [[CrossRef](#)]
4. Liao, M.C.; Huang, P.S.; Huang, T.C.; Tsai, M.Y. Backplate-reinforced structures for enhancing solder joint reliability of server CPU assembly under thermal cycling. *J. Mech.* **2021**, *37*, 693–703. [[CrossRef](#)]
5. Liao, M.C.; Huang, P.S.; Lin, Y.H.; Tsai, M.Y.; Huang, C.Y.; Huang, T.C. Measurements of thermally-induced curvatures and warpings of printed circuit board during a solder reflow process using strain gauges. *Appl. Sci.* **2017**, *7*, 739. [[CrossRef](#)]
6. Tsai, M.Y.; Wang, Y.W.; Liu, C.M. Thermally-induced deformations and warpings of flip-chip and 2.5D IC packages measured by strain gauges. *Materials* **2021**, *14*, 3723. [[CrossRef](#)] [[PubMed](#)]
7. Post, D.; Han, B.; Ifju, P. *High Sensitivity Moiré Experimental Analysis for Mechanics and Materials*; Springer: Berlin/Heidelberg, Germany, 1993.
8. Han, B.; Guo, Y.; Choi, H.C. Out-of-plane displacement measurement of printed circuit board by shadow moiré with variable sensitivity. In Proceedings of the 1993 ASME International Electronics Packaging Conference, Binghamton, NY, USA, 1 September 1993; pp. 179–185.
9. Hai, D.; Powell, R.E.; Hanna, C.R.; Ume, I.C. Warpage measurement comparison using shadow moiré and projection moiré methods. *IEEE Trans. Compon. Packag. Technol.* **2002**, *25*, 714–721.
10. Tsai, M.Y.; Chang, H.Y.; Pecht, M. Warpage analysis of flip-chip PBGA packages subject to thermal loading. *IEEE Trans. Device Mater. Reliab.* **2009**, *9*, 419–424. [[CrossRef](#)]
11. Tsai, M.Y.; Chen, Y.C.; Lee, S.W.R. Correlation between measurement and simulation of thermal warpage in PBGA with consideration of molding compound residual strain. *IEEE Trans. Compon. Packag. Technol.* **2008**, *31*, 683–690. [[CrossRef](#)]
12. Tsai, M.Y.; Ting, C.W.; Huang, C.Y.; Lai, Y.S. Determination of residual strains of the EMC in PBGA during manufacturing and IR solder reflow processes. *Microelectron. Reliab.* **2011**, *51*, 642–648. [[CrossRef](#)]
13. Suhir, E. Interfacial stresses in bimetal thermostats. *ASME J. Appl. Mech.* **1989**, *56*, 595–600. [[CrossRef](#)]
14. Suhir, E. Approximate evaluation of the elastic interfacial stresses in thin films with application to high -T_c superconducting ceramics. *Int. J. Solids Struct.* **1991**, *27*, 1025–1034. [[CrossRef](#)]
15. Tsai, M.Y.; Hsu, C.H.; Han, C.N. A note on Suhir’s solution of thermal stresses for a die-substrate assembly. *ASME J. Electron. Packag. Mar.* **2004**, *126*, 115–119. [[CrossRef](#)]
16. Tsai, M.Y.; Wang, Y.W. A theoretical solution for thermal warpage of flip-chip packages. *IEEE Trans. Compon. Packag. Manuf. Technol.* **2020**, *10*, 72–78. [[CrossRef](#)]
17. Wong, E.H.; Liu, J. Interface and interconnection stresses in electronic assemblies—A critical review of analytical solutions. *Microelectron. Reliab.* **2017**, *79*, 206–220. [[CrossRef](#)]

Disclaimer/Publisher’s Note: The statements, opinions and data contained in all publications are solely those of the individual author(s) and contributor(s) and not of MDPI and/or the editor(s). MDPI and/or the editor(s) disclaim responsibility for any injury to people or property resulting from any ideas, methods, instructions or products referred to in the content.